*Geomagnetism and Aeronomy, Vol. 42, No. 3, 2002, pp. 366–375. Translated from Geomagnetizm i Aeronomiya, Vol. 42, No. 3, 2002, pp. 383–393.*


# Simultaneous Radiophysical and Optical Measurements of the Ionospheric Response during the Large Magnetic Storm of April 6, 2000

**E. L. Afraimovich*, Ya. F. Ashkaliev**, V. M. Aushev**, A. B. Beletskii*, V. V. Vodyannikov**, L. A. Leonovich*, O. S. Lesyuta*, A. V. Mikhalev*, and A. F. Yakovets****

** Institute of Solar–Terrestrial Physics, Siberian Division, Russian Academy of Sciences, P.O. Box 4026, Irkutsk, 664033 Russia*

*** Institute of the Ionosphere, Ministry of Education and Science, Alma-Ata, Kazakhstan*

*e-mail: afra@iszf.irk.ru*

Received December 20, 2000

**Abstract**—The results of measuring the main parameters of the large-scale traveling disturbances of the midlatitude ionosphere at the maximum phase of the large magnetic storm of April 6, 2000, have been presented. The total electron content (TEC) changes have been obtained from the data of the GPS stations in Russia and Central Asia. The emission rates of the upper atmospheric OI 557.7- and 630-nm lines and the 360–410 and 720–830 nm spectral bands were measured simultaneously with TEC at the observatory of the Institute of Solar–Terrestrial Physics, Siberian Division, Russian Academy of Sciences, located near Irkutsk (51.9° N, 103.0° E), using the FENIX optical complex. The variations in the $O_2$ 866.5-nm emission rate have been obtained, using the MORTI complex, at the Institute of the Ionosphere, Ministry of Education and Science, Kazakhstan, located near Alma-Ata (43.2° N, 77.0° E). The variations in the critical frequency and altitude of the *F*2 layer were measured at the same institute with the help of a standard ionosonde. A data analysis indicated that the large-scale solitary wave with a duration of about 1 h and a not less than 5000-km-wide wavefront, formed as a result of the auroral disturbance, propagated equatorward over a distance of not less than 1000 km at an average velocity of ~200 m/s. The TEC disturbance, reflecting mainly a decrease in the electron concentration near the *F*2-layer maximum, correlates well with the emission rate, which increases in the optical range with a time shift different for different ionospheric altitudes.

## 1. INTRODUCTION

During strong geomagnetic storms, the main structures of the magnetosphere and ionosphere are subject to substantial changes in their localization and dynamics. Geophysical manifestations of extremely large magnetic storms are of special interest, because their probability of appearance is relatively low (not higher than four events in one 11-year solar cycle), and, therefore, representative data on the entire complex of processes interacting in the magnetosphere–ionosphere system is absent.

Large-scale traveling ionospheric disturbances (TID) with characteristic periods of 1–2 h and wavelengths of 1000–2000 km are one of the significant midlatitude manifestations of magnetic storms. Many works, including the detailed reviews [Hocke and Schlegel, 1996; Hunsucker, 1982], have been devoted to the studies of large-scale TID. It is assumed to be an established fact that such TID are the manifestation of acoustic gravity waves (AGW), whose regions of generation are located in the auroral zones of the Northern or Southern hemispheres. Therefore, the study of large-scale TID can yield important information about the processes proceeding in these zones under quiet and disturbed conditions.

Afraimovich *et al.* [2000] were the first to develop a method for determining large-scale TID characteristics based on calculating the spatial and temporal gradients of electron concentration with the use of three spaced GPS stations (GPS-array). The method was used to determine TID parameters during the large magnetic storm of September 25, 1998. The authors indicated that the large-scale solitary wave with a duration of ~1 h and wavefront width of not less than 3700 km, generated as a result of the auroral disturbance, propagated equatorward over a distance of not less than 2000–3000 km at an average velocity of ~300 m/s.

Yeh *et al.* [1994] studied the global response to the October 1989 magnetic storm, using the data of the ionosonde network. They observed low-latitude airglows over wide distances in the Northern and Southern hemispheres. The most pronounced manifestation of the storm is prolonged decreases in ionization at midlatitudes. During the storm main phase, the zone of disturbances extended toward the equator to a geomagnetic latitude lower than 10° and temporarily suppressed the equatorial anomaly.

A sufficiently large number of publications [Ishimoto *et al.*, 1986; Tinsley, 1979; Torr and Torr, 1984] have been devoted to the emission behavior in the midlatitude upper atmosphere during geomagnetic disturbances. The characteristic features of the spectral characteristics of the emissions in the mid- and low-latitude upper atmosphere during strong geomagnetic disturbances make it possible to combine such events in the class of "mid- and low-latitude auroras" [Rassoul *et al.*, 1993], which differ from "ordinary" auroras at high latitudes. These differences are, specifically, related to the appearance of $N_2^+$ 1N emissions in the airglow spectra of the midlatitude atmosphere [Ishimoto *et al.*, 1986; Tinsley *et al.*, 1984], substantial enhancement of the OI 630.0-nm emission, and predominance of atomic and ionic lines over molecular bands.

Rassoul *et al.* [1993] proposed a classification of several types of low-latitude airglows depending on the type of exciting particles (electrons, ions, and neutrals), predominant emissions, localization, and characteristic time scales. It is stated that several considered types of airglows, attesting, specifically, to the appearance of the mixture of energetic electrons and heavy particles, can often be simultaneously observed at middle and low latitudes. The 630-nm emission rate oscillations with a duration of 0.5–2 h are recorded during moderate geomagnetic disturbances at midlatitudes [Sahal *et al.*, 1988; Wiens *et al.*, 1991]. The midlatitude airglows observed during very strong magnetic storms ($Kp > 8$–9, $Dst > 300$ nT), for which the statistics of optical instrumental observations is limited, are of special interest.

This work is aimed at studying the response of the midlatitude ionosphere to the large magnetic storm of April 6, 2000, using the data of simultaneous radiophysical and optical measurements in Russia and Central Asia. In this case, special attention is paid to large-scale TID with a characteristic period of ~1 h.

## 2. DESCRIPTION OF THE GEOMAGNETIC CONDITIONS ON APRIL 6–7, 2000, AND GEOMETRY OF THE EXPERIMENT

Figure 1 presents (a) *K*-indices for Irkutsk station, (b) *Dst* variations of the geomagnetic field, and variations in the magnetic field *H* component at (c) Alma-Ata and (d) Irkutsk stations during the large magnetic storm of April 6–8, 2000. This storm had a pronounced sudden commencement (SSC) at 1642 UT. *K*-indices reached a value of eight at the storm maximum, and the sum of *K* was 48 in the course of a day. The *Dst* amplitude sharply increased to zero at 1600 UT on April 6 and then started rapidly decreasing and reached –319 nT at 2400 UT. The recovery phase began after that instant and continued until April 8. Vertical dashed lines in Fig. 1 mark SSC and the instant $t_{min}$ corresponding to the maximum value of the *dDst*/*dt* derivative (2000 UT).

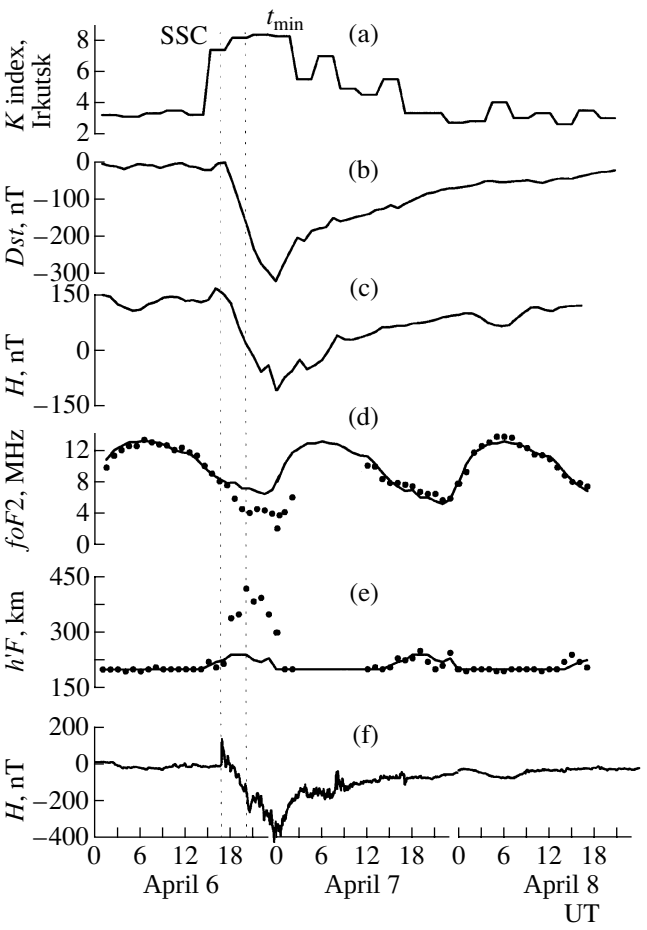


**Fig. 1.** Geomagnetic conditions in Irkutsk and Alma-Ata on April 6–8, 2000. (a) *K*-indices at Irkutsk station; (b) *Dst*-variations; variations in the magnetic field *H*-component at (c) Almaty and (f) Irkutsk stations; and variations in (d) *foF*2 and (e) *h'F* in Alma-Ata (heavy dots) and their median values (solid lines). Dashed vertical lines mark the instants of SSC and $t_{min}$ (the latter corresponds to the *d*/*dt*(*Dst*) maximum).

The geometry of the experiment is presented in Fig. 2 in the geographic frame of reference. The GPS stations are marked by heavy dots and small print. The LT values, corresponding to the given longitude interval, are plotted on the upper scale for the conventional instant of large-scale TID arrival at midlatitudes at 1900 UT (see Section 3). The positions of the MORTI (near Alma-Ata and SELE station) and FENIX (near Irkutsk and IRKT station) optical complexes are marked by rhombs and large print. The standard ionosonde, whose data are used in this work, was also installed in Alma-Ata.

Unfortunately, for the considered region, we managed to use the data of only 11 stations, whose coordinates are given in the table, in spite of the large number of GPS stations. It was necessary to detect large-scale TID at distances exceeding the anticipated wavelength (>1000 km) in order to reliably determine their characteristics. These arguments were also taken into account in selecting GPS stations.

General information about the experiment

| Ord. no. | Station | φ°, N | λ°, E | $t_{min}$, UT | $A_{min}$, TECU |
|---|---|---|---|---|---|
| 1 | YAKZ | 62.031 | 129.681 | 18.383 | –4.55 |
| 2 | ARTU | 56.430 | 58.560 | 19.000 | –4.94 |
| 3 | KSTU | 55.993 | 92.794 | 19.000 | –3.78 |
| 4 | ZWEN | 55.699 | 36.759 | 19.025 | –0.95 |
| 5 | IRKT | 52.219 | 104.316 | 19.683 | –2.28 |
| 6 | URUM | 43.808 | 87.601 | 21.017 | –0.81 |
| 7 | SELE | 43.179 | 77.017 | 20.958 | –0.71 |
| 8 | SHAS | 42.621 | 75.315 | 20.925 | –0.69 |
| 9 | KUMT | 41.863 | 78.190 | 20.992 | –0.91 |
| 10 | TRAB | 40.995 | 39.775 | 20.750 | –1.47 |
| 11 | KIT3 | 39.135 | 66.885 | 21.042 | –0.61 |
| 12 | FENIX | 52.9 | 103.0 | | |
| 13 | MORTI | 43.05 | 76.97 | | |

## 3. LARGE-SCALE TID CHARACTERISTICS ACCORDING TO THE GPS AND ALMATY IONOSONDE DATA

The GPS technique makes it possible to detect wave disturbances in the ionosphere on the basis of TEC phase measurements *I* at several spaced dual-frequency GPS receivers. The methods for deriving TEC relative changes from the measurements of the phase path increments of the GPS transionospheric radiosignal, caused by the ionosphere, are described in detail in many publications [Afraimovich *et al.*, 1998, 2000; Hofmann-Wellenhof *et al.*, 1992]. We present only the final formula for phase measurements:

$$I_0 = \frac{1}{40.308}\frac{f_1^2 f_2^2}{f_1^2 - f_2^2}[(L_1\lambda_1 - L_2\lambda_2) + \text{const} + nL], \quad (1)$$

where $L_1\lambda_1$ and $L_2\lambda_2$ are the radiosignal phase path increments due to the phase delay in the ionosphere (m), $L_1$ and $L_2$ are the numbers of complete phase reversals, $\lambda_1$ and $\lambda_2$ are the wavelengths (m) for frequencies $f_1$ and $f_2$, const is a certain unknown initial phase path (m), and $nL$ is the error in phase path determinations (m).

Below, we will use the total electron content unit (TECU), equal to $10^{16}$ m$^{-2}$, which is generally accepted in the literature.

The TEC series at the selected receiving stations, as well as the corresponding series of the angles of elevation $\theta(t)$ and azimuths $\alpha(t)$ of the beam to the satellite, calculated according to the CONVTEC program, which transforms Internet data (standard for the GPS RINEX system) into files, were used in our experiment as primary data for calculating large-scale TID characteristics. The continuous series of measurements $I_0(t)$ with a duration not shorter than 3 h are selected for determining TID parameters.

In order to eliminate variations in the regular ionosphere and the trends caused by the satellite motion, we got rid of the linear trend by preliminary smoothing the initial series, using the selected time window with a duration of ~60 min. The series of the angles of elevation $\theta(t)$ and azimuths $\alpha(t)$ of the beam to the satellite were used for determining the coordinates of subionospheric points.

For one and the same satellite (PRN25) and the time interval 1800–2200 UT at all stations from the tabulated set, the initial TEC series $I_0(t)$ were reduced to the vertical value, using the known technique [Klobuchar, 1986]

$$I = I_0 \cos\left[\arcsin\left(\frac{R_z}{R_z + h_{max}}\cos\theta\right)\right], \quad (2)$$

where $R_z$ is the Earth's radius, and $h_{max}$ = 400 km is the *F*2-layer maximum altitude.

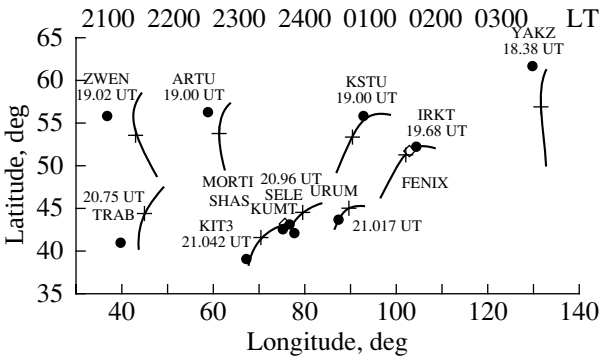


**Fig. 2.** Geometry of the experiment. Heavy dots and small print correspond to the GPS stations. Solid lines demonstrate the trajectories of motion of the subionospheric points. Crosses at the trajectories show the position of these points at the $t_{min}$ instants of TEC variations; the $t_{min}$ values in fractions of an UT hour are given nearby. LT is indicated above the figure. Rhombs and large print correspond to the position of the optical devices.

### *3.1. Large-Scale Traveling Ionospheric Disturbances According to the GPS Data*

The initial series $I(t)$ and the series $dI(t)$ with the eliminated trend are presented in Figs. 3 and 4. Because of the technical problems, for YAKZ station, we managed to use only data for the PRN30 satellite in the time interval 1700–2000 UT.

At virtually all GPS stations, $I(t)$ gradually decreases until a certain instant, which changes according to a station's position in the time interval 1900–2100 UT. Then, we can observe the deep and sharp

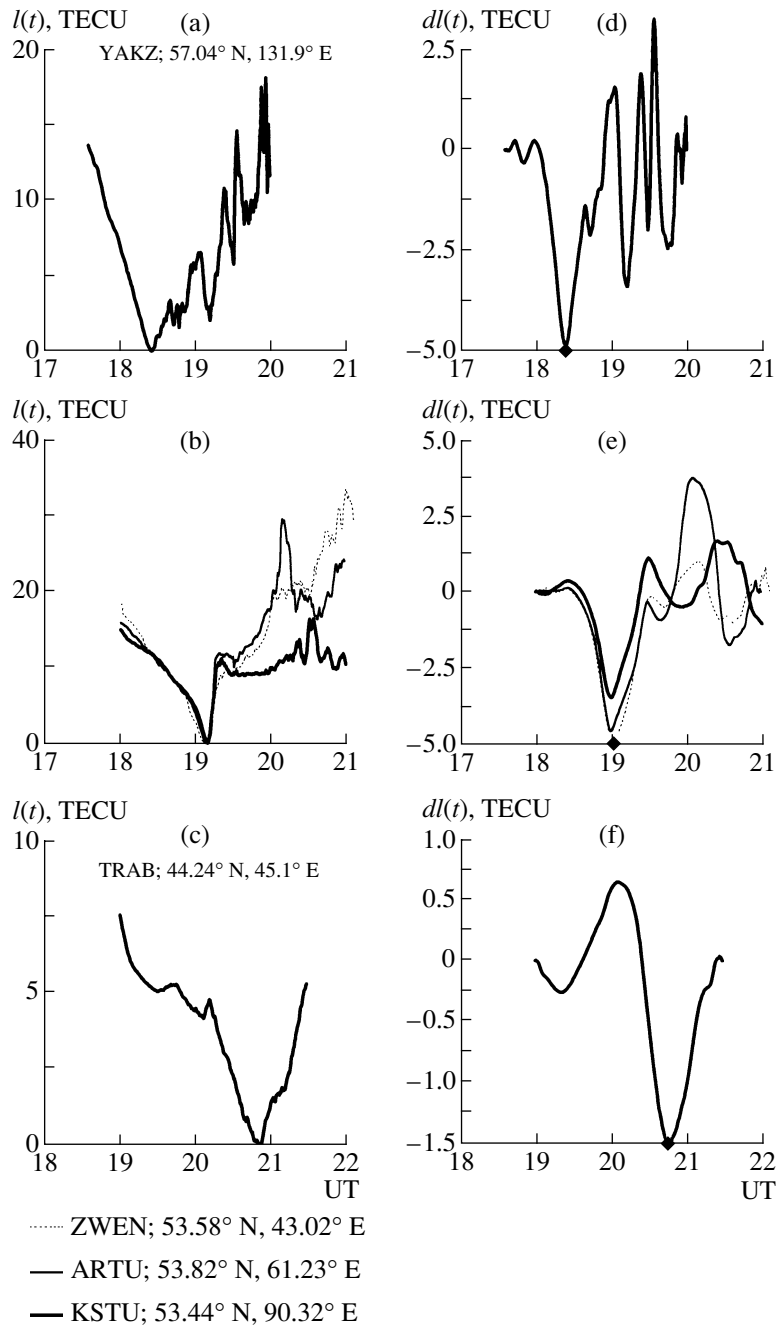


**Fig. 3.** Time variations in the oblique-incidence TEC, $I(t)$, for PRN25 at (b) GPS, ZWEN, ARTU, and KSTU and (c) TRAB stations; (e) and (f) TEC variations, $dI(t)$, without the trend and smoothed by a time window of 60 min. (a) and (d) Time variations $I(t)$ and $dI(t)$ for PRN30 at YAKZ station. Rhombs show the instants ($t_{min}$) of the $dI(t)$ minima.

minimum at $t_{min}$ (marked by rhombs on the $x$ axes in the right panels of Figs. 3, 4) and the pronounced drastic and rapid TEC variations after this instant.

One and the same satellite (PRN25) was selected for the entire set of stations (except for YAKZ), because the minimal beam angle of elevation $\theta(t)$ to this satellite exceeded 45° between 1900 and 2100 UT. This minimized a possible error in transforming the oblique TEC value into the vertical one due to the deviation of the TEC spatial distribution from the spherically symmetric distribution.

Solid curves in Fig. 2 indicate the trajectories of motion of subionospheric points for the PRN25 satellite (PRN30 for YAKZ) at an altitude of $h_{max}$ = 400 km. The positions of subionospheric points at the minima ($t_{min}$) of TEC variations are marked by crosses in the satellite orbits (see Figs. 3, 4); the $t_{min}$ values are given near crosses in UT hour fractions. The table gives the

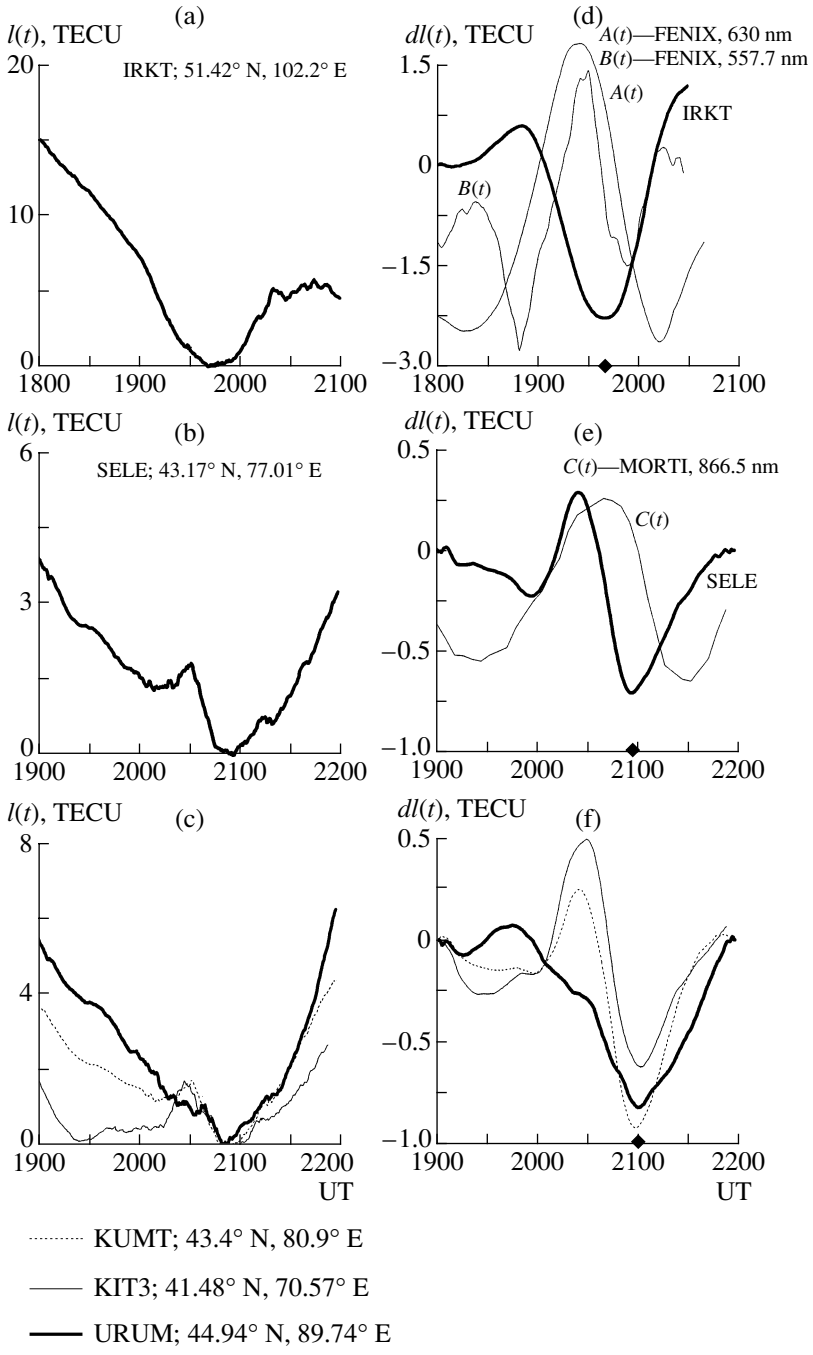


**Fig. 4.** The same as in Fig. 3 but for the GPS stations: (a) and (d) IRKT, (b) and (e) SELE, and (c) and (f) KUMT, KIT3, and URUM. Thin lines in panel (d) show the variations in the 630- and 557.7-nm emission rates ($A(t)$ and $B(t)$, respectively). Thin line in panel (e) indicates the variation in the 866.5-nm emission rate, $C(t)$.

$t_{min}$ values and corresponding $A_{min}$ amplitudes (in TECU) for a subionospheric point at each GPS station.

According to Fig. 2, the *dI* minimum was first observed at the subionospheric point for YAKZ at a latitude of 57° N (Fig. 3d). Then, it was almost simultaneously observed at a latitude of about 53° N (ZWEN, ARTU, and KSTU, Figs. 3b, 3e). These stations are located at a longitudinal distance of 47° E from one another; therefore, the obtained data indicate that the disturbance front width is not less than 5000 km. Forty minutes later, a similar disturbance was recorded at the subionospheric point for IRKT at 51.5° N (Figs. 4a, 4d). Approximately 2 h later, the disturbance $dI(t)$ of a

similar form was observed at latitudes of 40°–45° N, where TRAB (Figs. 3c, 3f), SELE (Figs. 4b, 4e), KIT3, KUMT, and URUM (Figs. 4c, 4f) stations are located.

Using the data of the table and Figs. 3 and 4, it is interesting to trace the variation in the TEC disturbance character with decreasing latitude of the subionospheric point. The disturbance $dI(t)$ amplitude $A_{min}$ pronouncedly decreases as the disturbance front moves southward from 5 TECU at the northern chain of stations to 1 TECU at the southern chain. Moreover, the rapid and drastic variations in $dI(t)$, typical of the high-latitude ionosphere, are observed after the abrupt decrease in $I(t)$. A similar fact was also reported by Afraimovich *et al.* [2000]. At the southern stations, such variations are substantially less pronounced.

These data can be interpreted in the following way. For the stations shown in the map northern sector (Fig. 2), in the indicated time interval (about 1900 UT), the beams to the satellite crossed the auroral zone southern boundary moving southward. Assuming that the disturbance front moved uniformly, then the delay of the disturbance appearance at the southern chain of stations (about 2 h) corresponds to a southward motion velocity of ~200 m/s.

Maeda and Handa [1980] and Whalen [1987] obtained similar results using the chain of ionosondes. In our case, the disturbance front width reaches 5000 km, which also agrees with the data obtained by Mikhalev [1997] and Whalen [1987].

Within the scope of this work, it is important that the value of a relative TEC variation (sharp decrease) was very large (from 15 to 20 TECU) along the entire front of the disturbance recorded at the chain of stations ZWEN, ARTU, KSTU, and YAKZ. According to the ideas generalized by Hunsucker [1982] and Ishimoto *et al.* [1986], such an extended and so abruptly overbalanced region of the atmosphere should become a source of powerful TID moving toward the equator. It is worth noting once again that the *Dst* derivative was maximal in this time interval (Fig. 1b), which agrees with a similar conclusion drawn by Ho *et al.* [1998].

### *3.2. Variations in the Critical Frequency and Virtual Height of the F2 Layer in Alma-Ata*

Figure 1d presents the variations in the *F*2-layer critical frequency (*foF2*) (heavy dots). Solid lines indicate the current medians determined by the method that uses the *foF2* values for three months [Wrenn *et al.*, 1987]. On the day before the magnetic storm, the magnetic conditions were quiet, and the *foF2* values were almost median. The main phase of the magnetic storm coincided with the Alma-Ata night. It is clear that the decrease in the critical frequency relative to the median values, which reflects the decrease in the electron concentration at the layer maximum, was observed shortly after the storm commencement. The difference between the *foF2* and median current values was maximal at an instant of *dDst*/*dt* maximum. The increase in *foF2*, which started at the appearance of the solar ionizing radiation, had a phase lag of approximately 2 h with respect to the increase in the median values. Unfortunately, data of sounding within seven hours after 0200 UT are absent because of technical problems. Therefore, the instant when the *foF2* current value became again similar to the median, is determined ambiguously.

The time variations in the virtual height *h'F* are shown in Fig. 1e by heavy dots. The variation in the current median value of *h'F* is shown by the solid line in the same figure. Figure 1e indicates that *h'F* started sharply increasing relative to its current median values simultaneously with a decrease in *foF2*. The height *h'F* recovered at 0100 UT. At that time, the critical frequency was equal to 6 MHz at a median value of 11 MHz. The sharp decrease in the critical frequency during the magnetic storm main phase agrees well with the drastic negative disturbance of TEC observed at the GPS stations (Fig. 4).

Thus, the considered magnetic storm was accompanied by an extremely considerable decrease in the electron content at the *F*-layer maximum, as a result of which *foF2* decreased by 4–5 MHz. The considerable increase in the virtual height of the *F* layer followed the decrease in the electron concentration.

## 4. OPTICAL MEASUREMENTS

### *4.1. Large-Scale Emission Rate Disturbances in Irkutsk*

The optical complex FENIX is located in the Geophysical observatory of the Institute of Solar–Terrestrial Physics, Siberian Division, Russian Academy of Sciences, at a distance of 100 km from Irkutsk (51.9° N, 103.0° E, geomagnetic latitude 41.0° N, $L$ = 2). This complex includes the four-channel zenithal photometer and a high-sensitivity television system based on a optoelectronic amplifier and CCD (charge coupled device) camera.

We performed the photometric measurements in the OI 557.7- and 630-nm emission lines and 360–410 and 720–830 nm spectral bands. The heights of the 557.7- and 630-nm emission glows under undisturbed conditions are 85–115 (with the emission maximum at 97 km) and 160–300 km (250–270 km), respectively. Under undisturbed conditions, the $O_2$ electron bands with the emission maximum at 97 km and the emission of hydroxyl (OH) molecules (scintillation heights 75–115 km, emission maximum at 85–90 km) are the main emission components in the spectral bands 360–410 and 720–830 nm, respectively.

The 557.7- and 630-nm emission lines were distinguished with the help of swinging interference light filters with characteristic halfwidths of 1–2 nm. The spectral bands 360–410 and 720–830 nm were distinguished with absorption light filters. The angular fields of view of the photometer channels were 4°–5°. The

absolute calibration of the measuring channels was performed in the individual previous periods against the reference stars and was subsequently controlled with the help of reference light sources. The photometer software made it possible to record the data of photometric channels with an averaging of 12 s. If the amplitudes of the appeared pulsed signals exceeded the specified threshold, the record was performed with a time resolution of 8 ms. During the magnetic storm of April 6, 2000, the measurements were carried out only with the four-channel zenithal photometer.

Figure 5 shows the variations in the upper atmospheric emission rate derived from the zenithal photometer data for April 6, 2000. The main characteristic feature of these variations was the increase in the 630.0-nm emission rate in the second half of the night by a factor of more than 20 (Fig. 5a, curve *1*) as compared to the emission values near midnight and on the previous geomagnetically quiet night of April 5, 2000 (Fig. 5a, curve *3*).

The dynamics of the increase in the 630.0-nm emission, which started after 1600 UT and continued at dawn, when the optical observations were terminated, included periodical disturbances in addition to the general tendency toward enhancement. In the 557.7-nm emission variations (Fig. 5a, curve *2*), we can observe an insignificant disturbance at ~1700 UT, coincident with the similar disturbance of the 630.0-nm emission, and a sharp (35%) increase in the emission rate, which coincides with the first phase of the maximal increase in the 630.0-nm emission rate.

The monotonous increase in the emission rate of the 360- to 410-nm spectral band with the superposition of irregular short-period disturbances, which is unusual for quiet geomagnetic conditions (Fig. 5b, curve *6* for the previous night of April 5, 2000), was observed beginning at 1700 UT (Fig. 5b, curve *4*). The emission rate in the 720- to 830-nm spectral band (Fig. 5b, curve *5*) monotonously decreased from 1400 UT to the beginning of geomagnetic disturbances (1600 UT) and stopped decreasing after 1600 UT.

It is interesting to compare these data with the TEC variations measured at the nearest station (IRKT). For comparison, Fig. 4d demonstrates (in relative units) the variations in the 630-nm, $A(t)$, and 557.7-nm, $B(t)$, emission rates, measured with the FENIX device and filtered out of the source data (Fig. 5a, curves *1* and *2*, respectively), as well as the TEC variations, $I(t)$. Figure 4d indicates that these variations very closely correlate with each other, and that the emission rate variations are in antiphase with the TEC variations. The maximum in the optical data leads the TEC variation minimum by approximately 12 min. The possible causes of such a phenomenon are discussed in Section 6.

### *4.2. Large-Scale Disturbances According to the Optical Data in Central Asia*

The optical complex MORTI (Mesopause Rotational Temperature Imager) was imported to Alma-Ata from Canada in 1997 in order to study a planetary wave dynamics in the region of mesopause within the scope of the PSMOS (Planetary Scale Mesopause Observing System) project. This complex was installed at an altitude of 2800 m above see level in the mountain region located at a distance of 20 km from Alma-Ata (43.05° N, 76.97° E). The MORTI instrumentation makes it possible to measure the rotational temperature and emission of the $O_2$ (0–1) 866.5-nm nightglow. The MORTI construction was described in detail by Misawa *et al.* [1984]. In this paper, we only briefly describe the MORTI instrumentation and its main specifications.

The MORTI construction includes a conical mirror, Fresnel lens, interference filter, photographic lens, and CCD camera. The MORTI optical axis is vertical. The conical mirror reproduces the observed ring-shaped region of the night sky at altitudes of 95–97 km with inner and outer ring diameters of 47 and 63 km, respectively. The interference filter is centered at a wavelength of 867.6 nm and has a bandpass of 0.27 nm. Thus, this filter makes it possible to transmit $O_2$ lines with different wavelengths from points located at different angular distances from the optical axis, forming six concentric rings (corresponding to six $O_2$ rotational lines) on the CCD-camera plane. The radial distribution of the image intensity includes information about the rotational temperature and integrated rate of the $O_2$ emission for the corresponding sky sector. The 5-min exposition makes it possible to measure the temperature and relative emission accurate to ±2 K and ±2%, respectively [Wiens *et al.*, 1991].

Dots in Fig. 6 demonstrate the variations in the $O_2$ 866.5-nm emission rate during the magnetic storm of April 6, 2000, versus UT, obtained at local night, using the MORTI of the Institute of the Ionosphere, Ministry of Education and Science, Kazakhstan. The solid line indicates (a) the rms trend and (b) the same series after the elimination of the rms trend. Figure 6a indicates that the considerable background variations in the emission were observed on April 6 until the instant which, according to the GPS data, is assumed to be the time of arrival of the solitary wave caused by the magnetic storm. The period of these variations was 2 h; therefore, it was possible to distinguish the solitary wave with a duration of about 1 h and the maximum at 20.7 UT against the background of these variations.

Figure 4e shows the variation in the 866.5-nm emission rate, $C(t)$, filtered out of the SELE source data (Fig. 6a) in the same way as the TEC data, $I(t)$, were processed. When comparing the results obtained from the GPS and MORTI data (Fig. 4e), we should note that the TEC data and MORTI $O_2$ emissions rather closely correlate with one another, though they are in antiphase:

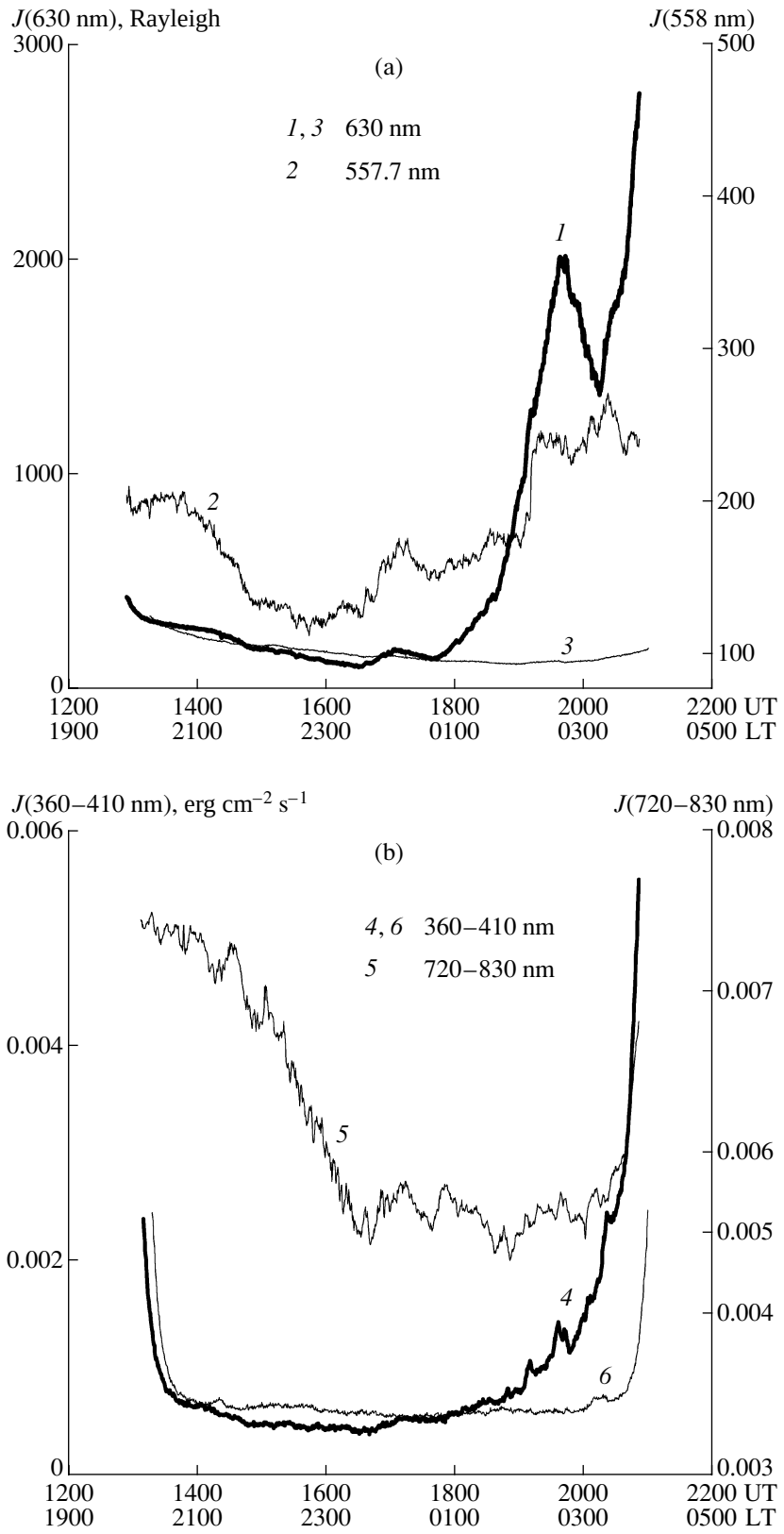


**Fig. 5.** (a) Variations in the atomic oxygen 630-nm (curve *1*) and 557.7-nm (curve *2*) emission rates; (b) variations in the nightglow emission rate in the spectral bands 360–410 (curve *4*) and 720–830 nm (curve *5*). Variations in the 630-nm (curve *3*) and 360- to 410-nm (curve *6*) emission rates on the magnetically quiet night of April 5, 2000.

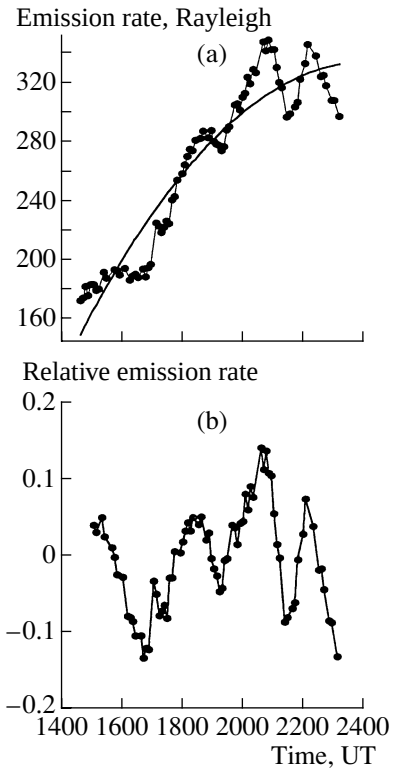


**Fig. 6.** (a) Variations in the $O_2$ 866.5-nm emission rate (heavy dots); solid line indicates the rms trend. (b) Relative variations in the same series upon eliminating the trend.

the $O_2$ line emission maximum leads the TEC minimum by approximately 18 min. However, in contrast to Irkutsk, the correlation between the TEC data and 866.5-nm emission rate at SELE is quite pronounced, but the phase relations are entirely different. Such a discrepancy can possibly be explained by taking into account the difference in the sensitivity ranges between the FENIX and MORTI devices.

## 5. DISCUSSION

The localization and dynamics of the main ionospheric trough (MIT), plasmasphere and plasmapause, and the zone of particle precipitation (auroral oval) and magnetospheric–ionospheric currents first of all affect the measured parameters discussed in the present paper. In the most disturbed periods, the plasmapause boundary can reach ultimate $L$ values in the range 1.7–2.5 [Khorosheva, 1987], MIT appears at 43° N invariant latitude [Annakuliev *et al.*, 1997], and the auroral oval boundary reaches corrected geomagnetic latitudes of 48° N (http://www.sec.noaa.gov/Aurora/index.html). For Irkutsk, the latter boundary is located at a corrected geomagnetic latitude of 47° N.

According to the NOAA 15 satellite data (http://sec.noaa.gov/pmap/pmapN.html), in the dawn of April 7, 2000, the auroral oval boundary (at a level of 0.1 erg $cm^{-2}$ $s^{-1}$) reached geographic latitudes of 56°–58° N in the considered longitudinal sector. Taking into account that the MIT width reaches several degrees, we can assume that at least its southern boundary reached the 52° N latitude in Eastern Siberia, where the optical observations were carried out. The aforesaid allows us to suppose that elements of the subauroral and, possibly, auroral ionosphere could be observed at the Irkutsk latitude during the April 6–7, 2000, magnetic storm. The data of optical observations also corroborate this assumption. The increased signal in the spectral band 360–410 nm after 1700 UT can be interpreted as the appearance of the $N_2^+$(1NG) emissions with a wavelength of 391.4 nm, which are usually observed in auroras as a result of the ionization of molecular nitrogen by precipitating electrons and energetic atoms or ions [Ishimoto *et al.*, 1986; Tinsley *et al.*, 1984].

In addition to the well-known increase in the 630-nm emission in midlatitude airglows, the 630-nm emission line maximum near 1930 UT, which anticorrelates (with a certain time delay) with TEC over the region of observations (Fig. 4d), is also of interest. A similar maximum of the 630-nm emission against a background of generally a growing emission rate was also observed near Irkutsk during the large magnetic storm of March 24–25, 1991 [Mikhalev, 1997]. If we relate the TEC minimum to the MIT propagation during the ring current enhancement at the storm initial phase, we can assume that the recorded maximum in the 630-nm emission develops in the MIT region where stable auroral red (SAR) arcs are usually observed [Rees and Roble, 1975].

In this sense, the data on SAR arcs over North America [Lobzin and Pavlov, 1998] are of interest. These authors in particular indicate that the weak airglow in the form of SAR arcs during strong magnetic disturbances can "become a low-latitude airglow" and cited the maximum SAR arc intensities in the 630-nm emission (2.2–4 kRayleighs) during large magnetic storms ($Dst$ < –200 nT). The 630-nm emission rates, recorded during the April 6, 2000, magnetic storm near Irkutsk, fall in this range. Other researchers (e.g., see [Khorosheva, 1987]) also identified SAR arcs with midlatitude airglows.

For SAR arcs, the increased population of the $^1D$ level of neutral oxygen results from the increased electron temperature at the altitudes of the $F2$ region and outer ionosphere. The latter is in turn related to the increased heat flux from the plasmasphere, where energy exchange takes place between the thermal plasma and ring current.

According to [Burns *et al.*, 1991], TEC directly depends on the $\frac{O}{(O_2 + N_2)}$ ratio. Therefore, an increase in $N_2$ results in a decrease in the local (and, consequently, integrated) electron concentration, which agrees with the obtained results (Fig. 4).

## 6. CONCLUSION

An analysis of the data indicated that the large-scale solitary wave with a duration of about 1 h and front width of not less than 5000 km, formed as a result of the auroral disturbance, propagated equatorward over a distance of not less than 1000 km at an average velocity of ~200 m/s. The TEC disturbance, reflecting mainly the decreased electron concentration in the vicinity of the *F*2 layer, closely correlates with the emission rate, increasing in the optical range with a time shift different at different ionospheric altitudes. We can assume that the elements of the subauroral ionosphere were observed at the Irkutsk latitude during the large magnetic storm. In Alma-Ata, the magnetic storm was accompanied by the unusually considerable decrease in the electron concentration at the *F*-layer maximum, which resulted in the 4–5 MHz decrease in the nighttime critical frequencies. The decrease in the electron concentration was accompanied by the increase in the layer virtual height.

## ACKNOWLEDGMENTS

We are grateful to E.A. Ponomarev and A.V. Tashchilin for their interest in this work, pieces of helpful advice, and active participation in discussions.

This work was supported by the INTAS (grant 99-1186), leading scientific schools of the Russian Federation (grant 00-15-98509), and the Russian Foundation for Basic Research, project no. 00-05-72026.

## REFERENCES

Afraimovich, E.L., Palamartchouk, K.S., and Perevalova, N.P., GPS Radio Interferometry of Travelling Ionospheric Disturbances, *J. Atmos. Solar–Terr. Phys.*, 1998, vol. 60, pp. 1205–1223.

Afraimovich, E.L., Kosogorov, E.A., Leonovich, L.A., *et al.*, Determining Parameters of Large-Scale Travelling Ionospheric Disturbances of Auroral Origin using GPS-Arrays, *J. Atmos. Solar-Terr. Phys.*, 2000, vol. 62, p. 553–565.

Annakuliev, S.K., Afonin, V.V., Deminov, M.G., and Karpachev, A.T., Empirical Formula for Positioning the Main Ionospheric Trough during a Magnetic Storm, *Geomagn. Aeron.*, 1997, vol. 37, no. 3, pp. 183–187.

Burns, A.G., Killen, T.L., and Roble, R.G., A Theoretical Study of Thermospheric Composition Perturbation during an Impulsive Geomagnetic Storm, *J. Geophys. Res.*, 1991, vol. 96, no. A8, pp. 153–167.

Ho, C.M., Iijima, B.A., Lindqwister, X.P., *et al.*, Ionospheric Total Electron Content Perturbations Monitored by the GPS Global Network during Two Northern Hemisphere Winter Storms, *J. Geophys. Res.*, 1998, vol. 103, pp. 26409–26420.

Hocke, K. and Schlegel, K., A Review of Atmospheric Gravity Waves and Travelling Ionospheric Disturbances: 1982–1995, *Ann. Geophys.*, 1996, vol. 14, pp. 917–940.

Hofmann-Wellenhof, B., Lichtenegger, H., and Collins, J., *Global Positioning System: Theory and Practice*, New York: Springer, 1992.

Hunsucker, R.D., Atmospheric Gravity Waves Generated in the High-Latitude Ionosphere. A Review, *Rev. Geophys.*, 1982, vol. 20, pp. 293–315.

Ishimoto, M., Torr, M.R., Richards, P.G., and Torr, D.G., The Role of Energetic $O^+$ Precipitation in a Mid-Latitude Aurora, *J. Geophys. Res.*, 1986, vol. 91, p. 5793.

Khorosheva, O.V., On the Relation between Discrete Forms of Polar Aurorae and Low-Latitude Auroral Red Arcs, *Geomagn. Aeron.*, 1987, vol. 27, no. 5, pp. 804–811.

Klobuchar, J.A., Ionospheric Time-Delay Algorithm for Single-Frequency GPS Users, *IEEE Trans. Aerospace Electronics System*, 1986, vol. 23(3), pp. 325–331.

Lobzin, V.V. and Pavlov, A.V., Association of the Brightness of Subauroral Red Arcs with Solar and Geomagnetic Activity, *Geomagn. Aeron.*, 1998, vol. 38, no. 4, pp. 49–61.

Maeda, S. and Handa, S., Transmission of Large-Scale TIDs in the Ionospheric *F*2-Region, *J. Atmos. Solar–Terr. Phys.*, 1980, vol. 42, pp. 853–859.

Mikhalev, A.V., Photometric Observation of Midlatitude Auroras Over South-East Siberia, *Abstracts 8th Scientific Assembly of IAGA with ICMA and STP Symposia*, Uppsala, August 4–15, 1997, p. 161.

Misawa, K., Takeuchi, I., and Aoyama, I., Apparent Progression of Intensity Variations of the Oxygen Red Line, *J. Atmos. Terr. Phys.*, 1984, vol. 46, no. 1, pp. 39–46.

Rassoul, H.K., Rohrbaugh, R.P., Tinsley, B.A., and Slater, D.W., Spectrometric and Photometric Observation of Low-Latitude Aurorae, *J. Geophys. Res.*, 1993, vol. 98, no. A5, pp. 7695–7709.

Rees, M.H. and Roble, R.G., Observations and Theory of the Formation of Stable Auroral Red Arcs, *Rev. Geophys. Space Phys.*, 1975, vol. 13, no. 1, p. 201.

Sahal, Y., Bittencourt, J.A., Takahasili, H., *et al.*, Multispectral Optical Observations of Ionospheric F-Region Storm Effects at Low Latitude, *Planet. Space Sci.*, 1988, vol. 36, no. 4, pp. 371–381.

Tinsley, B.A., Energetic Neutral Atom Precipitation during Magnetic Storm: Optical Emission, Ionization, and Energy Deposition at Low and Middle Latitudes, *J. Geophys. Res.*, 1979, vol. 84, p. 1855.

Tinsley, B.A., Rohrbaugh, R.P., Rassoul, H., *et al.*, Spectral Characteristics of Two Types of Low Latitude Aurorae, *Geophys. Res. Lett.*, 1984, vol. 11, no. 6, pp. 572–575.

Torr, M.R. and Torr, D.G., Energetic Oxygen in Mid-Latitude Aurora, *J. Geophys. Res.*, 1984, vol. 89, p. 5547.

Whalen, J.A., Daytime *F*-Layer Trough Observed on a Macroscopic Scale, *J. Geophys. Res.*, 1987, vol. 92, pp. 2571–2576.

Wiens, R.H., Zhang, S.P., Peterson, R.N., and Shepherd, G.G., MORTI: A Mesopause Oxygen Rotational Temperature Imager, *Planet. Space Sci.*, 1991, vol. 39, pp. 1363–1375.

Wrenn, G.L., Rodger, A.S., and Rishbeth, H., Geomagnetic Storm in the Antarctic F-Region, *J. Atmos. Terr. Phys.*, 1987, vol. 49, no. 9, pp. 901–913.

Yeh, K.C., Ma, S.Y., Lin, K.H., and Conkright, R.O., Global Ionospheric Effects of the October 1989 Geomagnetic Storm, *J. Geophys. Res.*, 1994, vol. 99, no. A4, pp. 6201–6218.